© 2014. Published by The Company of Biologists Ltd | Development (2014) 141, 1059-1063 doi:10.1242/dev.099994

RESEARCH REPORT

Embryonic bauplans and the developmental origins of facial diversity and constraint

Nathan M. Young[1,*], Diane Hu[1], Alexis J. Lainoff[1], Francis J. Smith[1,2], Raul Diaz[3,4], Abigail S. Tucker[5], Paul A. Trainor[3,4], Richard A. Schneider[1], Benedikt Hallgrímsson[2] and Ralph S. Marcucio[1]

ABSTRACT

A central issue in biology concerns the presence, timing and nature of phylotypic periods of development, but whether, when and why species exhibit conserved morphologies remains unresolved. Here, we construct a developmental morphospace to show that amniote faces share a period of reduced shape variance and convergent growth trajectories from prominence formation through fusion, after which phenotypic diversity sharply increases. We predict *in silico* the phenotypic outcomes of unoccupied morphospaces and experimentally validate *in vivo* that observed convergence is not due to developmental limits on variation but instead from selection against novel trajectories that result in maladaptive facial clefts. These results illustrate how epigenetic factors such as organismal geometry and shape impact facial morphogenesis and alter the locus of adaptive selection to variation in later developmental events.

KEY WORDS: Neural crest, Evolvability, Cleft lip

INTRODUCTION

Mammals, reptiles and avians exhibit tremendous phenotypic diversity as adults but are often remarkably similar to each other earlier in their embryonic development (Slack et al., 1993; Hall, 1996; Raff, 1996). The presence of such a 'phylotypic' stage of development suggests a causal relationship between conserved developmental mechanisms and mid-embryonic phenotypic convergence (Domazet-Lošo and Tautz, 2010); but whether, when and why such a period exists remains highly contested (Duboule, 1994; Raff, 1996; Hall, 1997; Bininda-Emonds et al., 2003; Kalinka and Tomancak, 2012). Resolving this issue is essential to understanding how development contributes to evolutionary change (Hallgrímsson et al., 2009), yet despite evidence for conserved genome and transcriptome-level expression within and between species (Roux and Robinson-Rechavi, 2008; Irie and Kuratani, 2011; Quint et al., 2012), comparable quantitative phenotypic data has lagged, hindering effective comparisons. Here, we use geometric morphometric analyses of shape to address this issue in the morphogenesis and growth of the amniote face.

The amniote face has its developmental origins in a shared embryonic organization or 'bauplan'. At its most basic, this bauplan consists of the frontonasal prominence (FNP) and the maxillary component of the first branchial arch (MxP), which first appear adjacent to the primordial brain, itself a simple flexed tube. Cranial neural crest (CNC) cells migrate from the dorsal neural tube to form the majority of the mesenchymal tissue of the MxP and FNP. Under the influence of reciprocal epithelial-mesenchymal signaling, the prominences grow in a highly choreographed manner, come into contact and fuse to form the primary palate, failure of which results in a cleft (Diewert and Lozanoff, 2002; Szabo-Rogers et al., 2008). The CNC differentiates into the connective tissues that comprise the facial cartilages and skeleton (Hall and Horstadius, 1988), and although the number, shape and size of facial elements varies widely among amniotes, their developmental origin and organization reflects this shared bauplan. In particular, the maxillary, zygomatic, jugal and quadratojugal bones are thought to be MxP derived, whereas the frontal, premaxilla and nasals are FNP derived (Morriss-Kay, 2001; Lee et al., 2004).

To address the presence, timing and nature of a conserved 'phylotypic' stage in amniote facial development, we first sampled embryos from each of the major amniote lineages (mammals, lizards and snakes, turtles, crocodilians and avians) and measured the location of anatomical landmarks that tracked the relative contributions of the FNP and MxP to the upper jaw of the adult skeleton (supplementary material Fig. S1). From these data, we next generated a shape 'morphospace' to describe variation in phenotype spanning the earliest period of embryonic facial morphogenesis through postnatal growth of the upper jaw, and quantified and compared divergence in shape across lineages and developmental time.

RESULTS AND DISCUSSION

Multivariate analysis of embryonic data indicated that species could be discriminated from one another at the earliest stages of facial morphogenesis, suggesting significant embryonic shape diversity (Fig. 1; supplementary material Tables S3, S4**)**. When analyzed as a developmental sequence, the majority of shape variation (78.0%) could be decomposed into three principal axes: a common pattern of progressive anterior facial outgrowth and mediolateral narrowing [PC1, 53.8% total shape variation (TSV)]; divergence in the relative proportions of maxilla to frontonasal (PC2, 15.5% TSV); and anteroventral extension of the FNP (PC3, 8.7% TSV) (Fig. 2A; supplementary material Fig. S2A-D). To compare developmental trajectories, we first noted that PC2 and PC3 were nonlinear with respect to PC1, a shape-defined measure associated with developmental age, and individual species had a better fit with a quadratic equation than a single linear regression [i.e. variance in residuals was significantly lower (Levene's test, $P<0.001$)]. Avian trajectories also appeared to progressively diverge from non-avians, such that average adult PC2 scores were significantly different (*t*-test, $P<0.001$). To estimate when these trajectories diverge, we estimated the convergence point from the quadratic equations of

[1]Department of Orthopaedic Surgery, University of California, San Francisco, San Francisco, CA 94110, USA. [2]Department of Cell Biology and Anatomy, University of Calgary, Calgary, AB T2N 4N1, Canada. [3]Stowers Institute of Medical Research, Kansas City, MO 64110, USA. [4]Department of Anatomy and Cell Biology, University of Kansas Medical Center, Kansas City, KS 66160, USA. [5]Department of Craniofacial Development and Stem Cell Biology, King's College London, London, SE1 9RT, UK.

*Author for correspondence (nathan.m.young@gmail.com)

Received 19 June 2013; Accepted 11 December 2013

Development (2014) doi:10.1242/dev.099994

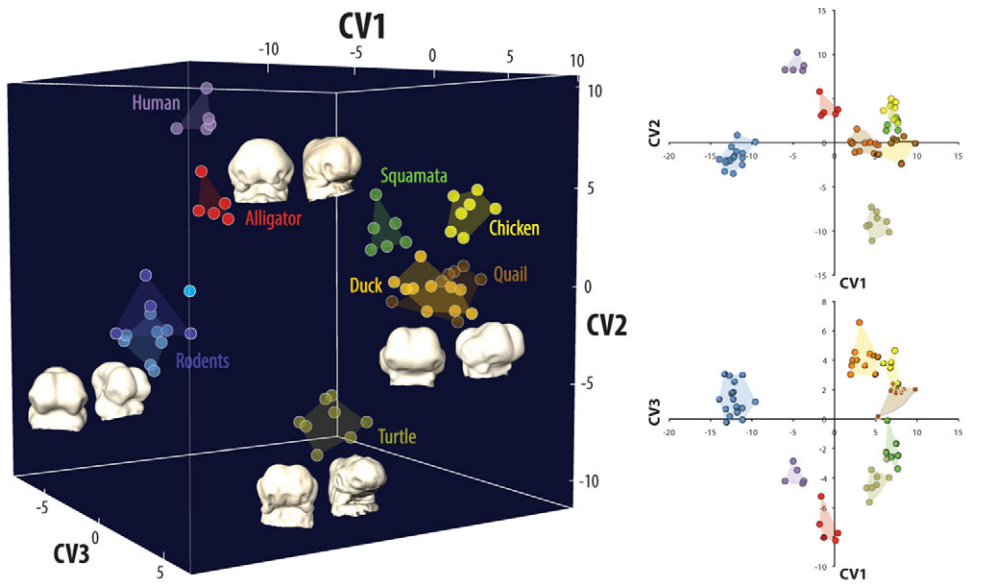

Fig. 1. Amniote embryos exhibit significant early diversity in shape. During early facial morphogenesis, phylogenetic variation in embryonic shape can be discriminated by the location of nasal placodes, the shape of the brain and FNP, and the orientation of the maxillaries. Representative early stage embryos are shown at the extremes of canonical variate (CV) axes in frontal and oblique views.

mean avian and non-avian trajectories (PC1~0.21), and the inflection point in the mean avian trajectory (PC1=0.07±0.01). This timeframe coincided with the period of facial fusion in avians (supplementary material Fig. S2A-C). Plotted against PC1, shape divergence is initially high, declines to its lowest point as trajectories converge around fusion (PC1=0.05-0.08) and then subsequently increases during fetal growth to reach its highest levels in adults (Fig. 2B; supplementary material Fig. S3).

From this analysis, amniote facial development can be divided into four common stages (Fig. 2A). In the first stage, the MxP is small and posteriorly located relative to the distal aspect of the face, and the nasal placodes are arranged on the lateral-ventral side of the flexed telencephalon. The MxP subsequently grows anteromedially, whereas the FNP becomes relatively smaller and the globular process rotates ventrally and posteriorly towards the distal MxP. During the next stage, these shape changes continue to drive the prominences towards each other such that lateral and distal most regions approximate, consistent with fusion of the primary palate. In the subsequent post-fusion stage of fetal growth, the entire face continues to elongate, but the trend in relative proportions of MxP and FNP (PC2), and ventral movement of the FNP (PC3) reverse. In adults, this distinction is most extreme in avians, where facial length is almost exclusively determined by the premaxilla, while the maxilla is highly reduced. By contrast, in the non-avian facial skeleton the premaxilla proportions

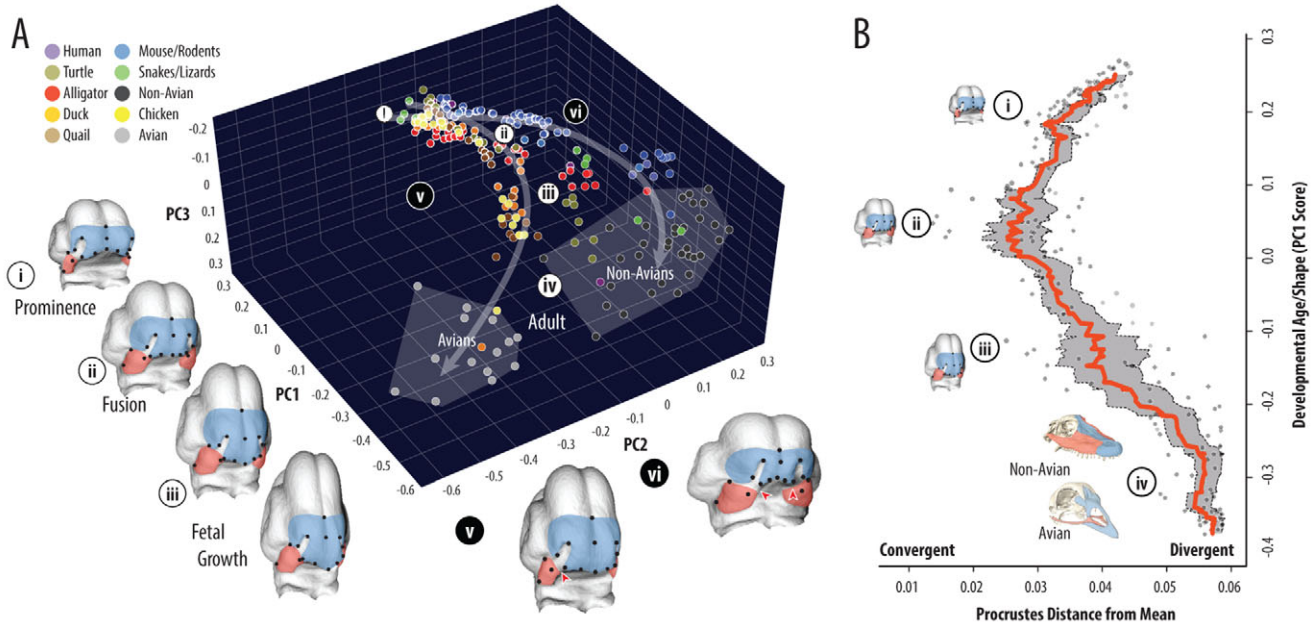

Fig. 2. Amniote shape variation and growth trajectories converge at prominence fusion and subsequently diverge. (A) Facial shape morphospace is defined by: anterior projection and midline convergence (PC1); relative proportions of the MxP (red) to FNP (blue) (PC2); and ventral projection of the FNP (PC3). PC1 tracks developmental age: (i) initial prominence outgrowth; (ii) contact and fusion of MxP and FNP; (iii) post-fusion prenatal growth; and (iv) adult skeleton. Avian and non-avian developmental shape trajectories (PC1-2 nonlinear regressions, arrows) converge (ii) before they diverge (iii), such that adult facial length is primarily maxillary derived in non-avians and frontonasal derived in avians (iv). Unoccupied regions of morphospace predict novel facial proportions, either FNP-dominant (v) or MxP-dominant (vi), both of which increase the likelihood of clefting (red triangles). (B) Average shape divergence (red line, gray shading=95% confidence interval) is lowest at prominence fusion (ii) and greatest in adults (iv).

Development (2014) doi:10.1242/dev.099994

vary from relatively small (e.g. turtles, humans) to proportionately large (e.g. ungulates), but facial length is always dominated by the maxilla (supplementary material Fig. S4).

This comparative analysis suggests that the most conserved period of amniote facial shape coincides with prominence fusion. To better understand this relationship, and in particular why avians diverge from non-avians around this developmental event but not earlier, we next used the comparative morphospace to infer rules of facial growth and predict potential but unrealized shapes. We found that deviations from conserved early trajectories resulted in increasing mismatch of relative prominence shape and size to facial length, and in avian lineages predicted a precocious outgrowth of the frontonasal, both of which increase the likelihood of clefts (Diewert and Lozanoff, 2002; Young et al., 2007) (Fig. 2A; supplementary material Fig. S2D). This result suggests that early trajectories are dictated in part by the geometric configuration and shape of constituent parts (i.e. maxillary, frontonasal, brain), particularly in the apposition of globular process of the frontonasal and the distal tip of the maxillary, and thus represent a potential epigenetic mechanism for phenotypic convergence. If this were the case, then prominences should be relatively intolerant to shape variation around the time of facial fusion, whether unilaterally (asymmetric) or bilaterally (symmetric) expressed.

To test this idea, we used the known function of the sonic hedgehog (SHH) signaling pathway in facial growth as a tool to experimentally manipulate relative prominence size and shape prior to fusion (Chai and Maxson, 2006). Although a number of pathways, such as bone morphogenetic protein (BMP), fibroblast growth factor (FGF) and Wingless (WNT) (Brugmann et al., 2007), may contribute to differential growth, SHH plays a crucial role in dorsoventral patterning, midline width variation, anterior outgrowth and palatal fusion (Marcucio et al., 2005; Hu and Marcucio, 2009; Young et al., 2010). When we compared embryonic stages corresponding to the period of maximal shape convergence, we found that *Shh* expression was localized to the distal tip and margins of the frontonasal, maxillary and primitive oral cavity (Fig. 3A-E). We hypothesized that selectively modulating *Shh* activity in one prominence, either by implanting a bead soaked in exogenous SHH-N protein to increase signaling or by electroporating a *Ptc*-Δ-loop construct to inhibit receptor activity and decrease signaling, would alter relative prominence growth and proportions, thereby increasing the incidence and severity of primary palatal clefts. As predicted, enhanced signaling increased maxillary or frontonasal proportions on the treated side, while decreased signaling had the opposite effect (Fig. 3F-O; supplementary material Fig. S5). Moreover, all experimental combinations altered the developmental trajectory into morphospace previously unoccupied by normal chickens and induced clefts of the primary palate (Fig. 3P).

Together these results demonstrate that amniote faces exhibit maximal phenotypic convergence at the mid-embryonic branchial arch stage, consistent with an hourglass model of development (Kalinka and Tomancak, 2012). Consistent with qualitative observations (Richardson, 1995), there is significant variation early in facial shape, notably in the location and orientation of the nasal placodes and MxP (Fig. 1; supplementary material Tables S2, S3). However, a full morphospace analysis suggests the shared amniote facial bauplan of initially independent outgrowths dictates that each species must confront the problem of fusion in order to generate an integrated and functional upper jaw. There are limited solutions to this problem; therefore, embryos must follow a developmental trajectory that maximizes the likelihood that distal facial prominences will contact at the appropriate time and place.

Experimental results similarly demonstrate that fusion is likely to be a strong selective filter against developmental shape variation. Normal variation at or near the time of fusion underestimates potential variation, as evidenced by the large number of genes known to contribute to primary cleft incidence and severity in humans (Dixon et al., 2011), many of which modulate the growth of prominences (Suzuki et al., 2009; Suazo et al., 2011). We targeted SHH signaling because of its known role in controlling mesenchymal growth zones,

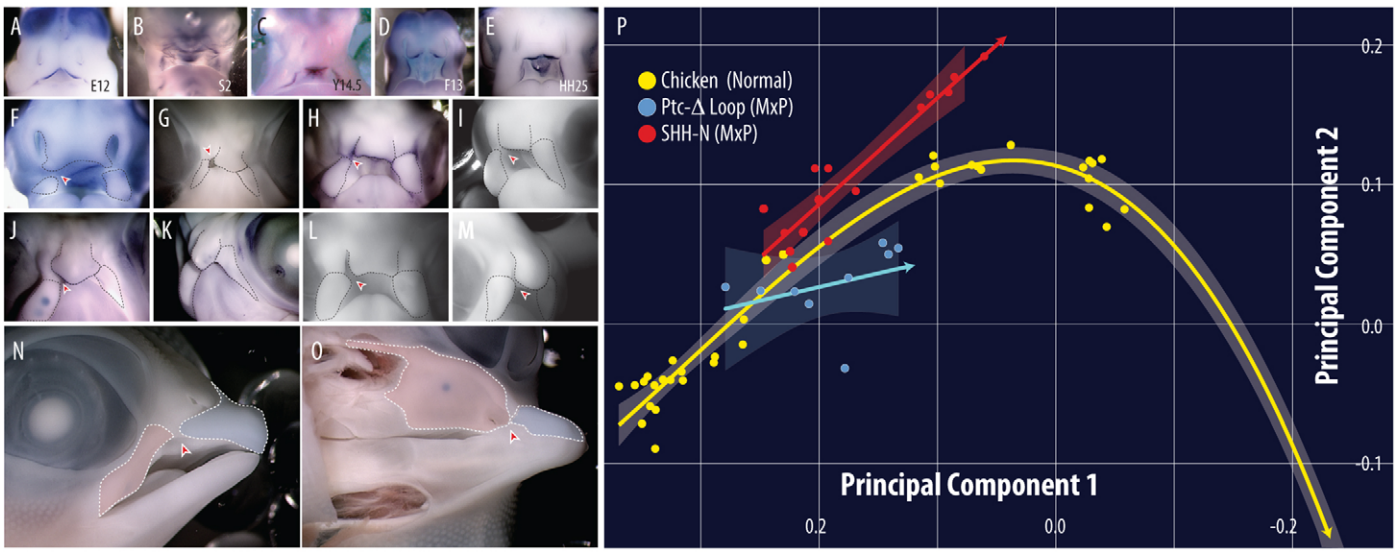

Fig. 3. Amniote sonic hedgehog (*Shh*) is similarly expressed at the time of fusion and altered signaling increases the likelihood of primary palatal clefts. *Shh* expression in (A) hamster (E12) (Theiler, 1989), (B) snake (stage 2) (Boback et al., 2012), (C) turtle (Y14.5) (Yntema, 1968), (D) alligator (F13) (Ferguson, 1985) and (E) chicken (HH25) (Hamburger and Hamilton, 1951). (F,G) Electroporation of Ptc-Δ-loop into the chicken maxillary alters prominence shape/size (right) relative to the control side (left) from 24 to 96 hours post-treatment and induces a primary palatal cleft (red arrowheads). Implantation of SHH-N into either the maxilla (H-K,N-O) or frontonasal region (L,M) expands the prominence and induces a cleft (red arrowheads). (P) Experimental trajectories deviate from normal into the morphospace predicted to induce a cleft (shading=95% confidence interval). Although performed on one side, we would predict that treatment on both sides would lead to a bilateral clefting phenotype.

Development (2014) doi:10.1242/dev.099994

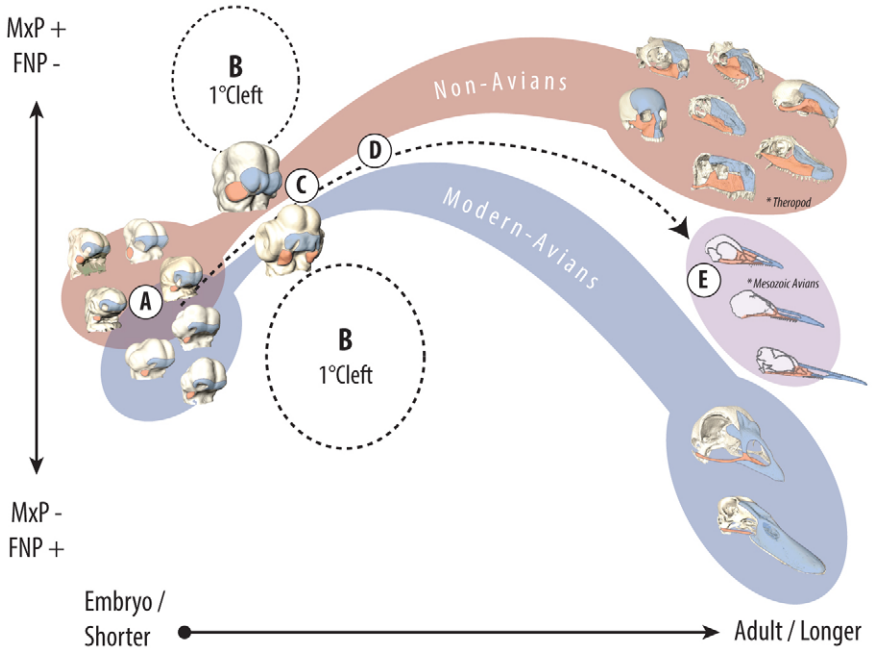

Fig. 4. Model of diversity and constraint in the amniote upper jaw. (A) Early amniote embryos exhibit distinct facial shapes. (B) Morphospace representing uncoordinated prominence growth relative to facial length enhances the likelihood of primary palatal clefts prior to fusion. (C) This constraint selects against facial shape variation around fusion and enhances phenotypic convergence. (D) Once fusion is complete, variation in post-fusion growth contributes to differences among extant avian and non-avian facial proportions. (E) The relationship of embryos to adults suggests that the modern avian beak evolved through a series of developmental shifts, including an extension of the post-fusion trajectory of the frontonasal skeletal derivatives (Bhullar et al., 2012). Potential ancestral taxa of avians, such as theropod dinosaurs, share the primitive amniote facial configuration (Marugán-Lobón and Buscalioni, 2004), but more recent Mesozoic avians are qualitatively intermediate with modern avians (Louchart and Viriot, 2011). In ancestral birds, diminution of maxillary proportions is associated with tooth loss (Louchart and Viriot, 2011), suggesting these traits either co-evolved or that reduced dental requirements freed maxillary derivatives to assume a smaller proportion of the jaw. Subsequent extinction of primitive transitional taxa created two discontinuous adaptive 'islands' in extant morphospace.

but similar predictions could be made of other genes or pathways that affect the relative growth of facial prominences and are implicated in cleft-lip etiology (Brugmann et al., 2007; Dixon et al., 2011). The relatively high incidence of clefting in humans (Diewert and Lozanoff, 2002) further suggests that natural variation at this crucial time period occurs, but is actively selected against. Observed phenotypic convergence at this stage is therefore the net result of selection against genetic variations that would induce both stage-inappropriate shape combinations and consequent structural defects detrimental to short-term jaw function and long-term individual fitness.

The divergence in both overall shape and growth trajectories after fusion supports the idea that the potential for clefts influences both phenotypic convergence, and when and how evolutionary diversity is generated (Fig. 4). We speculate that after the prominences fuse, the relative proportions of developmental components are free to vary more because the potential for clefting is no longer an issue. This post-fusion divergence is most obvious in the comparison between non-avian snouts, which are both maxillary and frontonasal derived, and avian beaks, which are primarily frontonasal derived. Associated with this divergent pattern is the location of the external nares, remnant markers of the nasal pits. In avians, the nares remain posteriorly located and facial length is primarily a result of premaxillary growth, whereas in non-avians the nasal aperture tracks the distal tip of the snout and length is dominated by the maxilla. Although some non-avians such as ungulates may have a proportionately large premaxilla, the modern avian beak occupies a novel and discontinuous region of morphospace. Even in non-avians, where skeletal correlates of the nares are posteriorly located, the underlying maxillary/frontonasal skeletal proportions remain in the primitive maxillary-dominant configuration (e.g. in whales, dolphins, tapirs, elephants), suggesting the avian condition is uniquely derived.

Together, these results demonstrate a period of convergent shape in the development of the amniote embryonic face associated with functional demands of prominence fusion. From a morphogenetic perspective, this period reflects epigenetic factors imposed by earlier developmental events rather than intrinsic limits to developmental variation. This suggests that periods of conserved gene expression during this developmental period may result from the way in which a shared bauplan impacts the selective landscape of morphospace. Although this analysis focuses on the face as a single organ system, we predict that epigenetic factors such as geometry and shape similarly constrain variation in other organs where the growth of simple structures must be coordinated to produce more complex shapes.

MATERIALS AND METHODS

Sample

We collected embryonic and fetal data for the following species (supplementary material Table S1). (1) Mammals: *Mus musculus* (mouse) (*n*=41), *Meriones unguiculatus* (gerbil) (*n*=2), *Rattus norvegicus* (rat) (*n*=4), *Mesocricetus auratus* (hamster) (*n*=7), *Homo sapiens* (human) (*n*=6). (2) Snakes and lizards: *Elaphe guttata* (python royal) (*n*=2), *Chamaeleo calyptratus* (veiled chameleon) (*n*=6). (3) Turtles: *Trachemys scripta* (red-eared slider) (*n*=21). (4) Crocodilians: *Alligator mississippiensis* (alligator) (*n*=24). (5) Avians: *Gallus gallus* (chicken) (*n*=22), *Coturnix coturnix* (quail) (*n*=21) and *Anas platyrhynchos* (white pekin duck) (*n*=24). With the exception of humans, embryos were incubated (reptiles, avians) or gestated (mammals) for a set time, then dissected and fixed in 4% paraformaldehyde (PFA)/5% glutaraldehyde. Samples were scanned at a resolution of 5-25 µm in a ScanCo 40 micro-computed tomography scanner. Human shape data were reconstructed from scanned serial sections of the Carnegie series of human embryonic development at an effective resolution of 5-20 µm. For each specimen, a three-dimensional (3D) model was reconstructed in the software *Amira 5.4* (Mercury Systems).

Morphospace analysis

We identified 17 landmarks on the maxillary and frontonasal prominences in prenatal samples and associated locations on skeletal derivatives of a broad sample of adult crania (supplementary material Fig. S1, Table S2). Three-dimensional landmark coordinates (x,y,z) were identified and recorded in *Landmark* (*v. 3.0*) (Wiley et al., 2005) and analyzed in *MorphoJ* (*v.1.05d*) (Klingenberg, 2011). Intraobserver error from repeated measurement of the same specimens was not significant. Procrustes superimposition transformed landmark configurations into a common scale-free shape space. Procrustes data of early embryonic samples (prominence stage before fusion) were ordinated via Canonical Variates Analysis (CVA) to estimate distance measures among species with

significance of shape differences determined via resampling. Principal Components Analysis (PCA) of the full developmental series was used to describe a morphospace of coordinated shape variation. To visualize the morphospace and generate shape predictions, a thin-plate spline algorithm was used to warp a 3D object fitted to the mean landmark configuration in *EVAN toolbox v. 1.40* (http://www.evan-society.org/node/23). We calculated shape divergence as the average Procrustes distance from the mean shape of the total sample.

Gene expression

Dioxigenin (DIG)-labeled riboprobes for Sonic hedgehog (*Shh*) were synthesized for each species (mouse, python, turtle, alligator and chicken). The mouse probe was used for all rodent species, whereas the chicken probe was used on all avian species. Whole-mount *in situ* hybridization was performed following established protocols (Moustakas, 2007; Hu and Marcucio, 2009).

Experimental manipulations

To upregulate SHH signaling, SHH-N protein beads (800 mg/ml) were placed into one side of the mesenchyme of the maxillary or frontonasal prominence of a chicken embryo at HH20. To downregulate SHH signaling, a constitutively active Patched (*Ptc*)-Δ-loop construct was unilaterally electroporated into the ectoderm of the maxillary prominence at stage HH15-16. Embryos were collected from both 48-72 hours post-treatment and at 12 days to assess for skeletal clefts. For morphometric analysis, each side (treated and normal) was treated as a single individual and compared with the original dataset (right and left).

Acknowledgements

We thank R. Elsey and the Louisiana Department of Wildlife and Fisheries for alligator embryos, and J. Moustakas for alligator and turtle *Shh* riboprobe plasmids. J. Cork provided data from the Virtual Human Embryo. The authors thank the three anonymous reviewers, members of the Marcucio laboratory, D. Noden and K. Katsura for feedback, suggestions and comments that improved the manuscript.

Competing interests

The authors declare no competing financial interests.

Author contributions

N.Y., B.H. and R.M. designed the research. N.Y. and B.H. analyzed the data. N.Y., R.M. and D.H. conceived the experiments. D.H. performed the experiments. N.Y., A.L., F.S. and R.D. collected the data. A.T., P.T. and R.S. contributed embryological specimens and reagents. All authors contributed to the writing of the paper.

Funding

This research was funded by National Institutes of Health/The National Institute of Dental and Craniofacial Research (NIH/NIDCR) [F32DE018596 to N.M.Y., R01DE019638 and R01DE021708 to R.S.M. and B.H., R01DE016402 to R.A.S. and R01DE016082 to P.A.T.], by the Stowers Institute for Medical Research (P.A.T.) and by the Natural Sciences and Engineering Research Council of Canada (NSERC) [238992-12 to B.H.]. Deposited in PMC for release after 12 months.

Supplementary material

Supplementary material available online at
http://dev.biologists.org/lookup/suppl/doi:10.1242/dev.099994/-/DC1

References

Bhullar, B. A., Marugán-Lobón, J., Racimo, F., Bever, G. S., Rowe, T. B., Norell, M. A. and Abzhanov, A. (2012). Birds have paedomorphic dinosaur skulls. *Nature* **487**, 223-226.

Bininda-Emonds, O. R. P., Jeffery, J. E. and Richardson, M. K. (2003). Inverting the hourglass: quantitative evidence against the phylotypic stage in vertebrate development. *Proc. Biol. Sci.* **270**, 341-346.

Boback, S. M., Dichter, E. K. and Mistry, H. L. (2012). A developmental staging series for the African house snake, Boaedon (Lamprophis) fuliginosus. *Zoology* **115**, 38-46.

Brugmann, S. A., Goodnough, L. H., Gregorieff, A., Leucht, P., ten Berge, D., Fuerer, C., Clevers, H., Nusse, R. and Helms, J. A. (2007). Wnt signaling mediates regional specification in the vertebrate face. *Development* **134**, 3283-3295.

Chai, Y. and Maxson, R. E., Jr (2006). Recent advances in craniofacial morphogenesis. *Dev. Dyn.* **235**, 2353-2375.

Diewert, V. M. and Lozanoff, S. (2002). Animal models of facial clefting: experimental, congenital, and transgenic. In *Understanding Craniofacial Anomalies: Etiopathogenesis of Craniosynostoses and Facial Clefting* (ed. M. M. Mooney and M. I. Siegel) pp. 251-272. New York, NY: Wiley-Liss.

Dixon, M. J., Marazita, M. L., Beaty, T. H. and Murray, J. C. (2011). Cleft lip and palate: understanding genetic and environmental influences. *Nat. Rev. Genet.* **12**, 167-178.

Domazet-Lošo, T. and Tautz, D. (2010). A phylogenetically based transcriptome age index mirrors ontogenetic divergence patterns. *Nature* **468**, 815-818.

Duboule, D. (1994). Temporal colinearity and the phylotypic progression: a basis for the stability of a vertebrate Bauplan and the evolution of morphologies through heterochrony. *Dev. Suppl.* **1994**, 135-142.

Ferguson, M. J. (1985). Development. In *Biology of the Reptilia* (ed. C. Gans, F. Billet and P. F. A. Maderson), pp. 329-491. New York, NY: John Wiley and Sons.

Hall, B. K. (1996). Bauplane, phylotypic stages, and constraint: Why there are so few types of animals. *Evol. Biol.* **29**, 215-261.

Hall, B. K. (1997). Phylotypic stage or phantom: is there a highly conserved embryonic stage in vertebrates? *Trends Ecol. Evol.* **12**, 461-463.

Hall, B. K. and Horstadius, S. (1988). *The Neural Crest*. London: Oxford University Press.

Hallgrímsson, B., Jamniczky, H., Young, N. M., Rolian, C., Parsons, T. E., Boughner, J. C. and Marcucio, R. S. (2009). Deciphering the Palimpsest: Studying the Relationship Between Morphological Integration and Phenotypic Covariation. *Evol. Biol.* **36**, 355-376.

Hamburger, V. and Hamilton, H. L. (1951). A series of normal stages in the development of the chick embryo. *J. Morphol.* **88**, 49-92.

Hu, D. and Marcucio, R. S. (2009). Unique organization of the frontonasal ectodermal zone in birds and mammals. *Dev. Biol.* **325**, 200-210.

Irie, N. and Kuratani, S. (2011). Comparative transcriptome analysis reveals vertebrate phylotypic period during organogenesis. *Nat. Commun.* **2**, 248-254.

Kalinka, A. T. and Tomancak, P. (2012). The evolution of early animal embryos: conservation or divergence? *Trends Ecol. Evol.* **27**, 385-393.

Klingenberg, C. P. (2011). MorphoJ: an integrated software package for geometric morphometrics. *Mol. Ecol. Resour.* **11**, 353-357.

Lee, S. H., Bédard, O., Buchtová, M., Fu, K. and Richman, J. M. (2004). A new origin for the maxillary jaw. *Dev. Biol.* **276**, 207-224.

Louchart, A. and Viriot, L. (2011). From snout to beak: the loss of teeth in birds. *Trends Ecol. Evol.* **26**, 663-673.

Marcucio, R. S., Cordero, D. R., Hu, D. and Helms, J. A. (2005). Molecular interactions coordinating the development of the forebrain and face. *Dev. Biol.* **284**, 48-61.

Marugán-Lobón, J. and Buscalioni, A. D. (2004). Geometric morphometrics in macroevolution: morphological diversity of the skull in modern avian forms in contrast to some theropod dinosaurs. In *Morphometrics: Applications in Biology and Paleontology* (ed. A. M. T. Elewa), pp. 157-173. Berlin: Springer-Verlag.

Morriss-Kay, G. M. (2001). Derivation of the mammalian skull vault. *J. Anat.* **199**, 143-151.

Moustakas, J. E. (2007). *The Evolution and Development of Skeletogenic Mesenchyme in Reptiles*. PhD dissertation, University of California Berkeley, CA, USA.

Quint, M., Drost, H.-G., Gabel, A., Ullrich, K. K., Bönn, M. and Grosse, I. (2012). A transcriptomic hourglass in plant embryogenesis. *Nature* **490**, 98-101.

Raff, R. A. (1996). *The Shape of Life: Genes, Development and the Evolution of Animal Form*. Chicago, IL: University of Chicago Press.

Richardson, M. K. (1995). Heterochrony and the phylotypic period. *Dev. Biol.* **172**, 412-421.

Roux, J. and Robinson-Rechavi, M. (2008). Developmental constraints on vertebrate genome evolution. *PLoS Genet.* **4**, 1-10.

Slack, J. M., Holland, P. W. H. and Graham, C. F. (1993). The zootype and the phylotypic stage. *Nature* **361**, 490-492.

Suazo, J., Tapia, J. C., Santos, J. L., Castro, V. G., Colombo, A. and Blanco, R. (2011). Risk variants in *BMP4* promoters for nonsyndromic cleft lip/palate in a Chilean population. *BMC Med. Genet.* **12**, 163-171.

Suzuki, S., Marazita, M. L., Cooper, M. E., Miwa, N., Hing, A., Jugessur, A., Natsume, N., Shimozato, K., Ohbayashi, N., Suzuki, Y. et al. (2009). Mutations in *BMP4* are associated with subepithelial, microform, and overt cleft lip. *Am. J. Hum. Genet.* **84**, 406-411.

Szabo-Rogers, H. L., Geetha-Loganathan, P., Nimmagadda, S., Fu, K. K. and Richman, J. M. (2008). FGF signals from the nasal pit are necessary for normal facial morphogenesis. *Dev. Biol.* **318**, 289-302.

Theiler, K. (1989). *The House Mouse: Atlas of Embryonic Development*. New York, NY: Springer-Verlag.

Wiley, D. F., Amenta, N., Alcantara, D. A., Ghosh, D., Kil, Y. J., Delson, E., Harcourt-Smith, W., Rohlf, F. J., St. John, K. and Hamann, B. (2005). Evolutionary Morphing. In *Proceedings of IEEE Visualization 2005*, pp.431-438. doi: 10.1109/VISUAL.2005.1532826

Yntema, C. L. (1968). A series of stages in the embryonic development of Chelydra serpentina. *J. Morphol.* **125**, 219-251.

Young, N. M., Wat, S., Diewert, V. M., Browder, L. W. and Hallgrímsson, B. (2007). Comparative morphometrics of embryonic facial morphogenesis: implications for cleft-lip etiology. *Anat. Rec. (Hoboken)* **290**, 123-139.

Young, N. M., Chong, H. J., Hu, D., Hallgrímsson, B. and Marcucio, R. S. (2010). Quantitative analyses link modulation of sonic hedgehog signaling to continuous variation in facial growth and shape. *Development* **137**, 3405-3409.

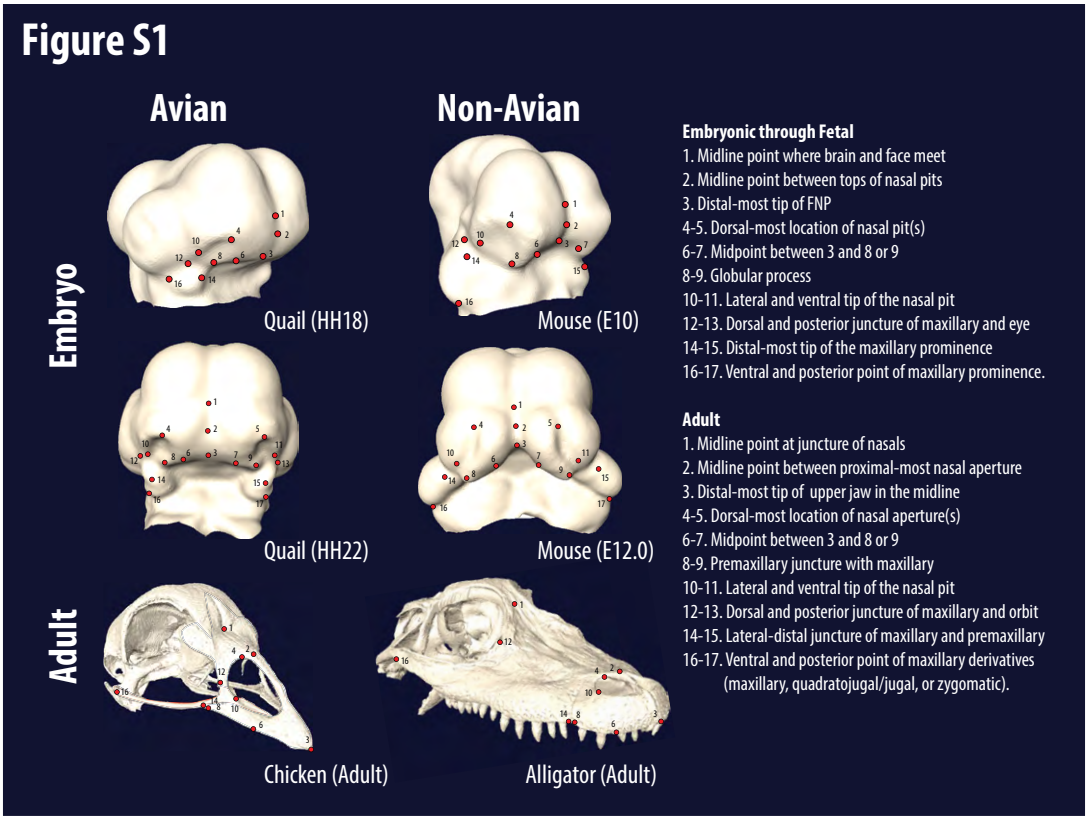

Figure S1: Morphometric Landmarks. Representative embryos and adults are shown with the location of landmarks and their descriptions. Surface landmarks and skeletal landmarks are considered to be homologous locations for the purpose of morphometric analysis. To choose these landmarks we tracked surface features of the facial prominences from prominence outgrowth to fusion and later fetal growth. Skeletal derivatives in adults were matched to surface fetal structures using generalized descriptions and published fate mapping (e.g., assuming that the distal tip of the embryonic frontonasal process corresponds to the distal tip of the adult upper jaw).

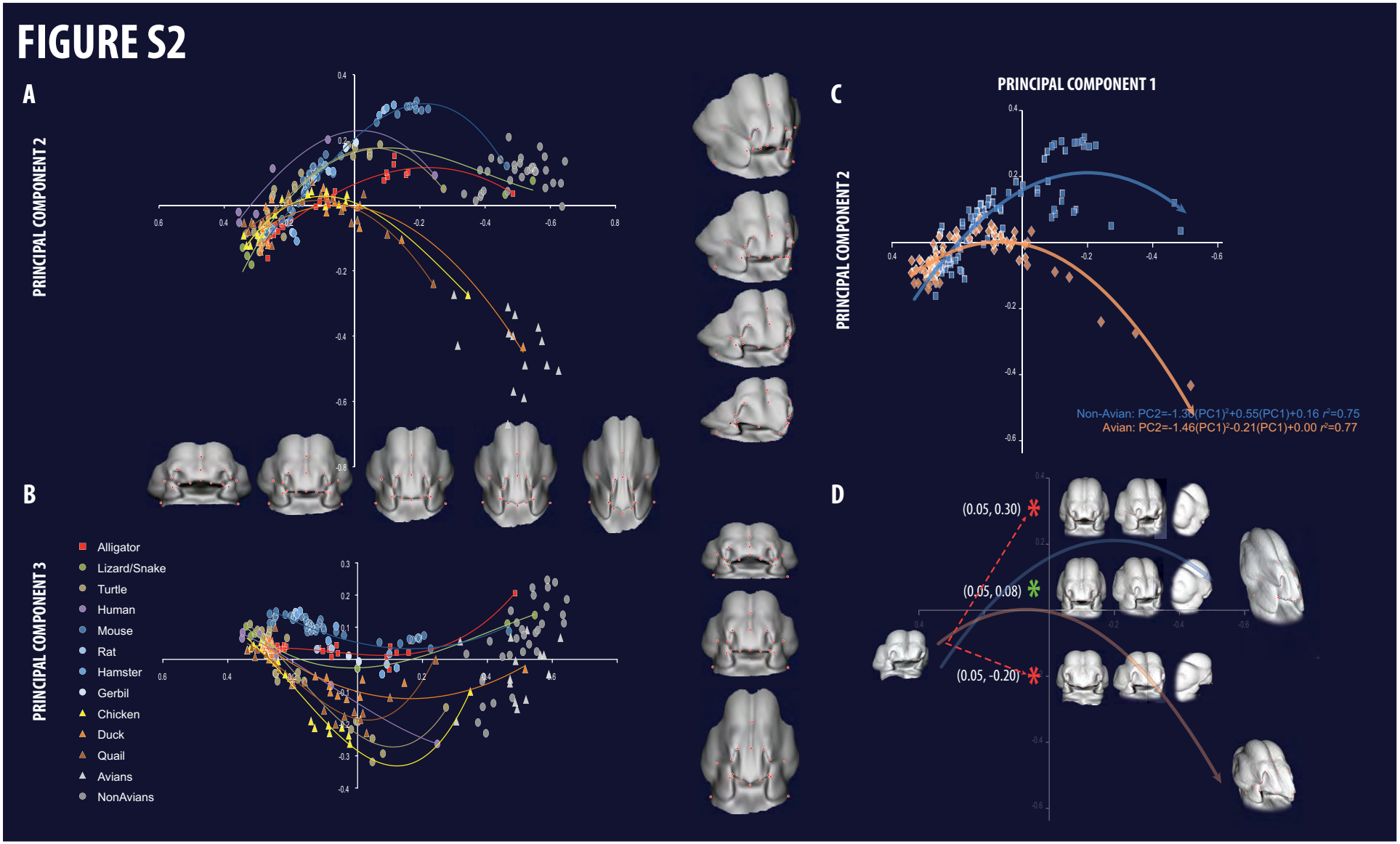

Figure S2. PCA axes in two-dimensional scatterplots. **A**. PC1 versus PC2. **B**. PC1 versus PC3. **C**. Estimated average non-avian (blue squares) and avian (red diamonds) PC1-2 developmental trajectories (lines). **D**. Estimated landmark configurations and embryo morphologies of trajectories above, within, and below amniote averages at common PC1 (developmental age/facial length).

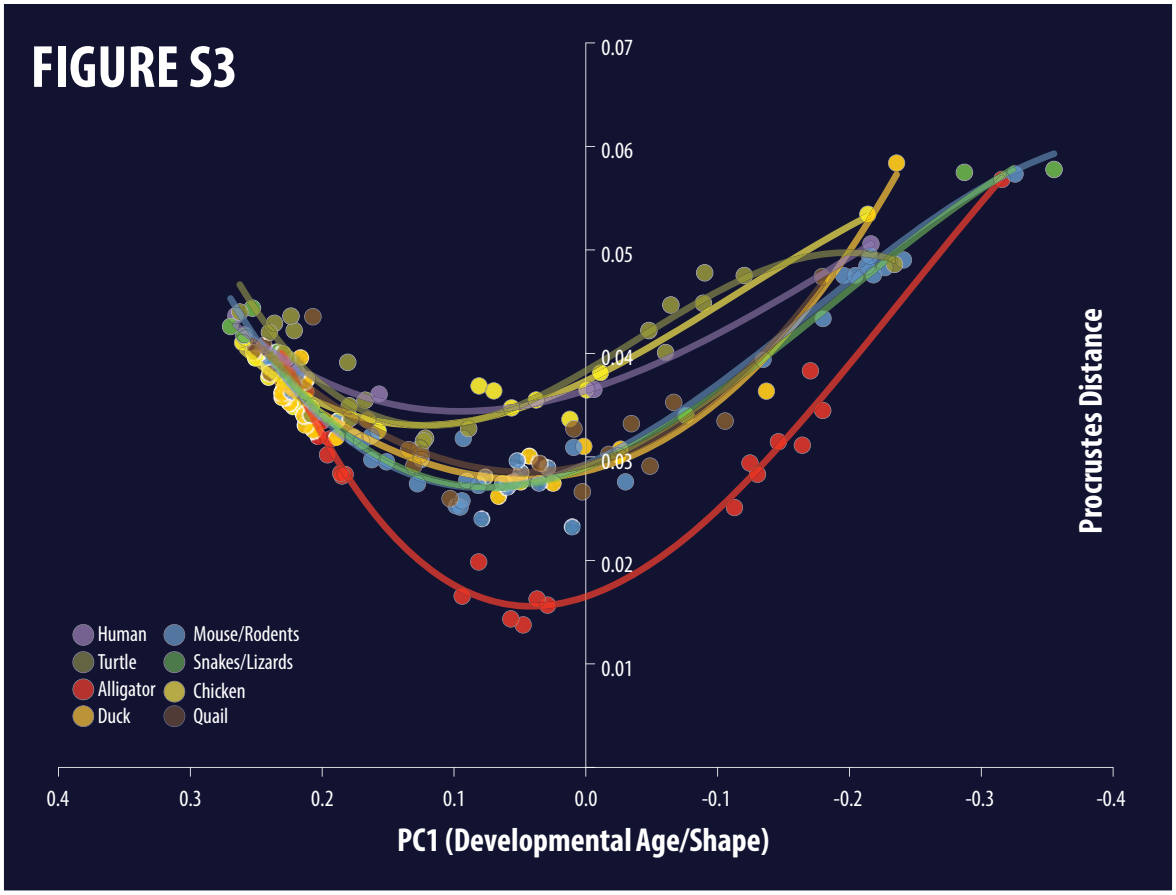

Figure S3. Average Procrustes distance for each species. Data from Figure 1B plotted for individual species. All species are most convergent with the average facial shape at or near the time of facial primordial fusion, after which shape diversity steadily increases.

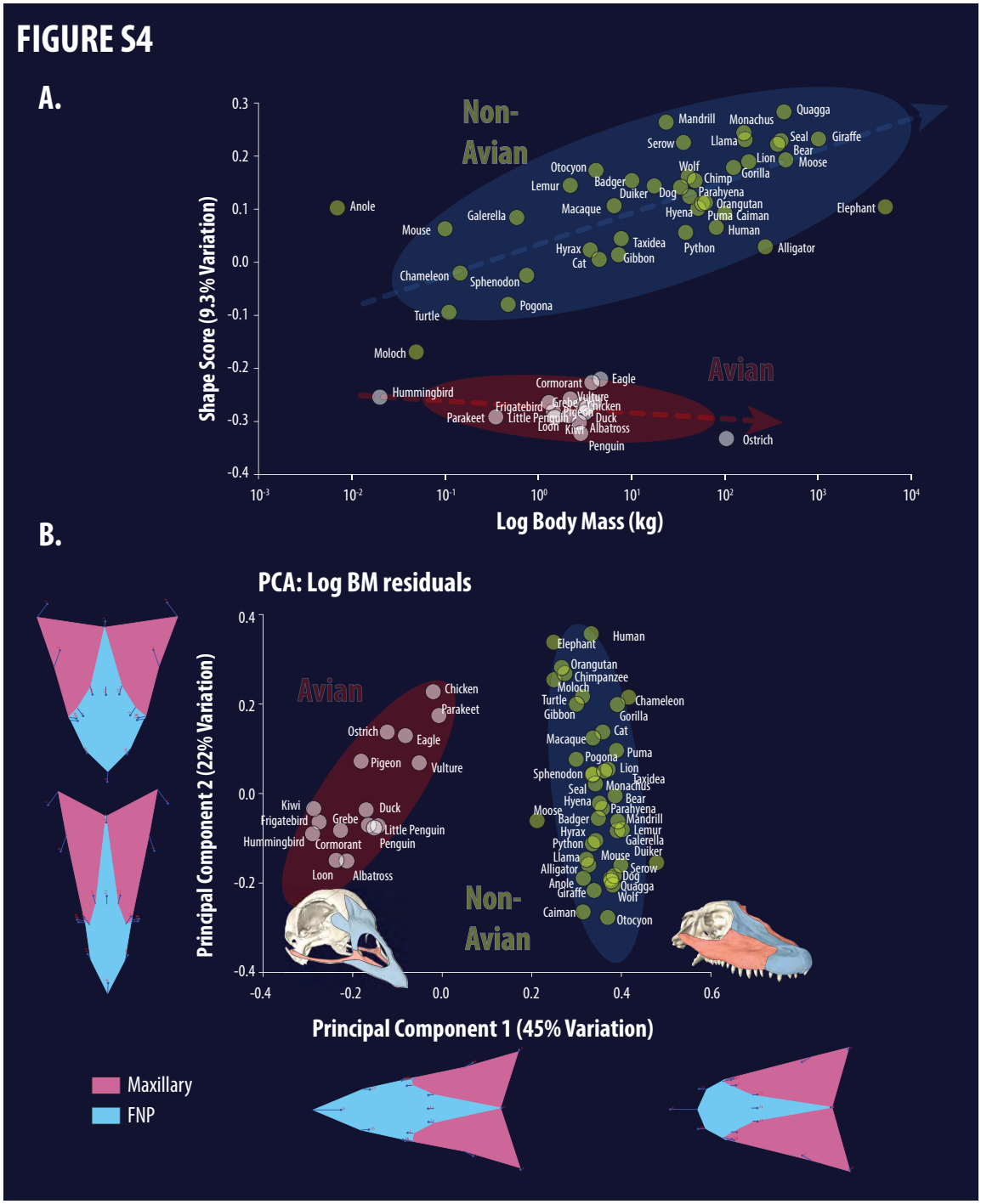

Figure S4. Allometry and shape comparison in adult amniote skulls. **A**. Multivariate regression of log body mass (kg) on shape reveals divergence in shape-size relationship between non-avian and avian amniote adults. **B**. PCA of body-mass/shape residuals from (**A**) demonstrates that the relative proportions of the maxillary and FNP-derivatives (PC1) separate avians and non-avians even when accounting for allometry, while in both groups longer skulls tend to be narrower (PC2). Mean landmark configurations are shown in dorsal view with vectors showing direction and magnitude of eigenvectors. Faces color-coded according to developmental derivatives (maxillary=red, FNP=blue).

Figure S5

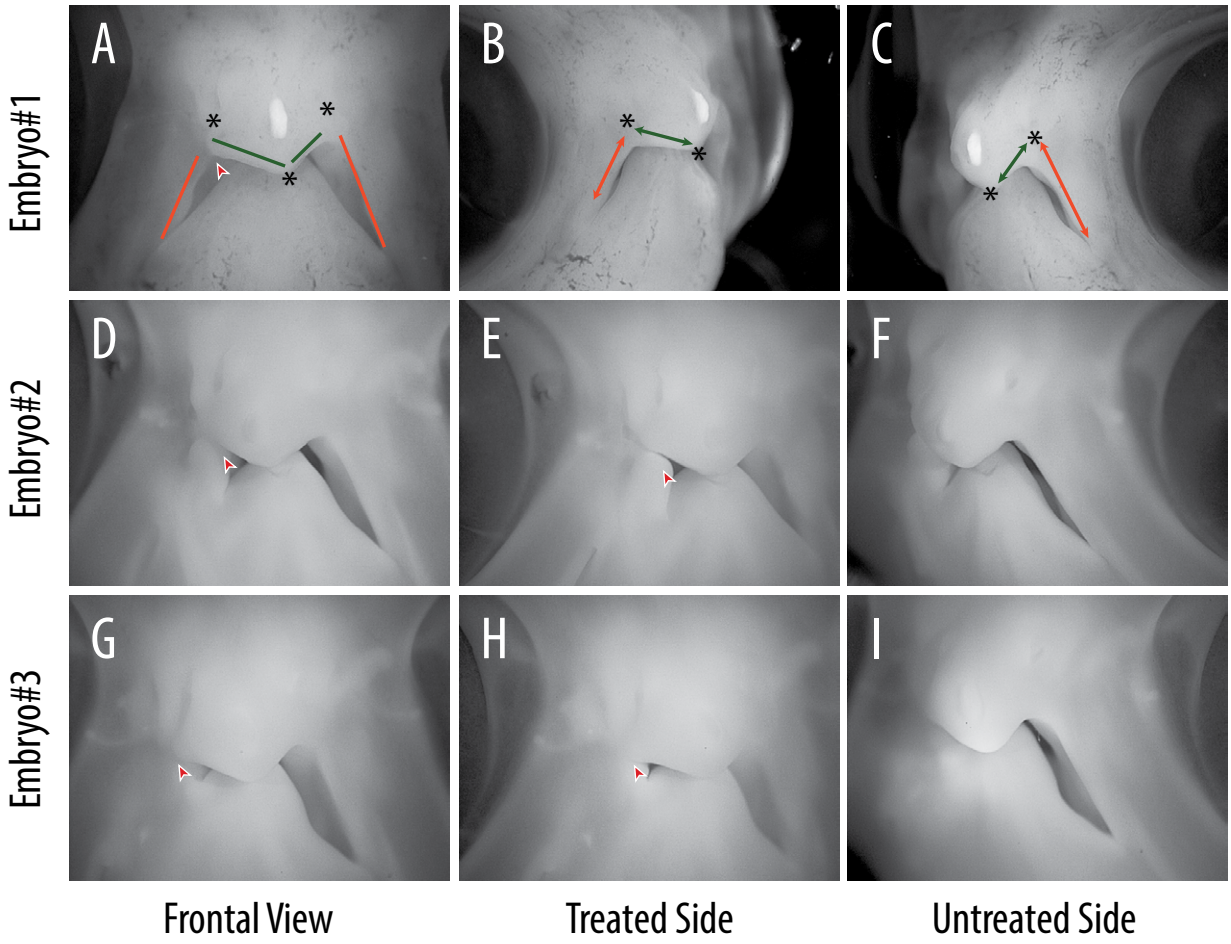

Figure S5. Additional experimental outcomes. We performed a dual experimental treatment in which both a SHH-N bead was placed in the FNP and Ptc-Δ-loop was electroporated into the maxillary at HH15-16. All embryos (N=3) exhibited reduced maxillaries and expanded FNPs (compare arrows on treated versus untreated sides), as well as clefts of the primary palate (red arrows) compared to untreated sides.

Table S1: Embryonic sample age composition (Hrs=hours incubation, CS=Carnegie stage, TS=tail somites, Th=Theiler stage).

Common	Order	Species	Unit	Age	N
Alligator	Crocodilia	*Alligator mississippiensis*	Hrs	216	1
Alligator	Crocodilia	*Alligator mississippiensis*	Hrs	240	2
Alligator	Crocodilia	*Alligator mississippiensis*	Hrs	264	2
Alligator	Crocodilia	*Alligator mississippiensis*	Hrs	288	3
Alligator	Crocodilia	*Alligator mississippiensis*	Hrs	312	3
Alligator	Crocodilia	*Alligator mississippiensis*	Hrs	360	3
Alligator	Crocodilia	*Alligator mississippiensis*	Hrs	384	3
Alligator	Crocodilia	*Alligator mississippiensis*	Hrs	456	3
Alligator	Crocodilia	*Alligator mississippiensis*	Hrs	480	2
Alligator	Crocodilia	*Alligator mississippiensis*	Hrs	528	2
Ball python	Reptilia	*Elaphe guttata*	Hrs	192	1
Chameleon	Reptilia	*Chameleo chameleon*	Hrs	168	6
Turtle	Testudines	*Trachemys scripta*	Hrs	168	5
Turtle	Testudines	*Trachemys scripta*	Hrs	192	3
Turtle	Testudines	*Trachemys scripta*	Hrs	264	4
Turtle	Testudines	*Trachemys scripta*	Hrs	288	3
Turtle	Testudines	*Trachemys scripta*	Hrs	360	3
Turtle	Testudines	*Trachemys scripta*	Hrs	384	3
Human	Mammalia	*Homo sapiens*	CS	14	1
Human	Mammalia	*Homo sapiens*	CS	15	1
Human	Mammalia	*Homo sapiens*	CS	16	1
Human	Mammalia	*Homo sapiens*	CS	17	1
Human	Mammalia	*Homo sapiens*	CS	18	1
Mouse	Mammalia	*Mus musculus* (C57bl)	TS	1	1
Mouse	Mammalia	*Mus musculus* (C57bl)	TS	2	3
Mouse	Mammalia	*Mus musculus* (C57bl)	TS	3	1
Mouse	Mammalia	*Mus musculus* (C57bl)	TS	7	1
Mouse	Mammalia	*Mus musculus* (C57bl)	TS	8	1
Mouse	Mammalia	*Mus musculus* (C57bl)	TS	10	2
Mouse	Mammalia	*Mus musculus* (C57bl)	TS	11	2
Mouse	Mammalia	*Mus musculus* (C57bl)	TS	12	1
Mouse	Mammalia	*Mus musculus* (C57bl)	TS	13	2
Mouse	Mammalia	*Mus musculus* (C57bl)	TS	15	2
Mouse	Mammalia	*Mus musculus* (C57bl)	TS	16	2
Mouse	Mammalia	*Mus musculus* (C57bl)	Th	11.5	15
Mouse	Mammalia	*Mus musculus* (C57bl)	Th	12.5	8
Rat	Mammalia	*Rattus norvegicus*	Th	12	1
Rat	Mammalia	*Rattus norvegicus*	Th	13	2
Rat	Mammalia	*Rattus norvegicus*	Th	14	1
Hamster	Mammalia	*Mesocricetus auratus*	Th	9	2
Hamster	Mammalia	*Mesocricetus auratus*	Th	10	2
Hamster	Mammalia	*Mesocricetus auratus*	Th	11	3
Gerbil	Mammalia	*Meriones unguiculatus*	Th	16	2

Chicken	Aves	*Gallus gallus*	Hrs	84	3
Chicken	Aves	*Gallus gallus*	Hrs	96	4
Chicken	Aves	*Gallus gallus*	Hrs	108	1
Chicken	Aves	*Gallus gallus*	Hrs	120	2
Chicken	Aves	*Gallus gallus*	Hrs	132	2
Chicken	Aves	*Gallus gallus*	Hrs	144	2
Chicken	Aves	*Gallus gallus*	Hrs	156	6
Duck	Aves	*Anas platyrhynchos*	Hrs	102	3
Duck	Aves	*Anas platyrhynchos*	Hrs	120	8
Duck	Aves	*Anas platyrhynchos*	Hrs	138	2
Duck	Aves	*Anas platyrhynchos*	Hrs	144	1
Duck	Aves	*Anas platyrhynchos*	Hrs	150	1
Duck	Aves	*Anas platyrhynchos*	Hrs	162	2
Duck	Aves	*Anas platyrhynchos*	Hrs	168	1
Duck	Aves	*Anas platyrhynchos*	Hrs	174	1
Duck	Aves	*Anas platyrhynchos*	Hrs	180	3
Duck	Aves	*Anas platyrhynchos*	Hrs	186	1
Duck	Aves	*Anas platyrhynchos*	Hrs	204	1
Quail	Aves	*Coturnix coturnix*	Hrs	72	1
Quail	Aves	*Coturnix coturnix*	Hrs	84	2
Quail	Aves	*Coturnix coturnix*	Hrs	96	4
Quail	Aves	*Coturnix coturnix*	Hrs	114	3
Quail	Aves	*Coturnix coturnix*	Hrs	120	3
Quail	Aves	*Coturnix coturnix*	Hrs	126	1
Quail	Aves	*Coturnix coturnix*	Hrs	144	5
Quail	Aves	*Coturnix coturnix*	Hrs	168	1
Quail	Aves	*Coturnix coturnix*	Hrs	216	1

Table S2: Adult Sample and Body Masses (NSF Digital Morphology Library at the University of Texas, Austin [NSF], www.digimorph.org, Ohio University Visible Interactive Alligator [VIA], www.oucom.ohiou.edu/dbms-witmer/3D_gator.htm, Kyoto University Primate Research Institute Digital Morphology Museum, [KU], www2.pri.kyoto-u.ac.jp/dmm/WebGallery/index.html).

Species (common name)	Group	3D Source	BM (kg)	log BM
Anas platyrhynchos (white pekin duck)	Avian	NSF	3.2	0.51
Apteryx australis (kiwi)	Avian	NSF	3.3	0.52
Brotogeris chrysopterus (parakeet)	Avian	NSF	0.35	-0.46
Columba livia (pigeon)	Avian	Paper	2.1	0.32
Coragyps atratus (black vulture)	Avian	NSF	2.2	0.34
Diomedea immutabilis (albatross)	Avian	NSF	2.75	0.44
Eudyptula minor (little penguin)	Avian	NSF	1.5	0.18
Fregata magnificens (frigatebird)	Avian	NSF	1.45	0.16
Gallus gallus (chicken)	Avian	NSF	2.94	0.47
Gavia immer (common loon)	Avian	NSF	4	0.60
Haliaeetus leucocephalus (bald eagle)	Avian	NSF	4.65	0.67
Patagona gigas (hummingbird)	Avian	NSF	0.02	-1.70
Phalacrocorax sp. (cormorant)	Avian	NSF	3.75	0.57
Podilymbus podiceps (grebe)	Avian	NSF	1.3	0.11
Spheniscus demersus (penguin)	Avian	NSF	2.85	0.45
Struthio camelus (ostrich)	Avian	NSF	104	2.02
Alces alces (moose)	Non-avian	NSF	450	2.65
Alligator mississippiensis (alligator)	Non-avian	VIA	271.5	2.43
Anolis carolinensis (green anole)	Non-avian	NSF	0.007	-2.15
Caiman sp. (caiman)	Non-avian	KU	100	2.00
Canis familiaris (dog)	Non-avian	KU	33.5	1.53
Canis lupus (wolf)	Non-avian	KU	40.5	1.61
Capricornis crispus (serow)	Non-avian	NSF	36	1.56
Cephalophus sp. (duiker)	Non-avian	NSF	17.5	1.24
Chameleo chameleon (chameleon)	Non-avian	NSF	0.145	-0.84
Elephas maximus (Asian elephant)	Non-avian	NSF	5250	3.72
Equus quagga (quagga)	Non-avian	KU	430.5	2.63
Felis concolor (puma)	Non-avian	KU	62	1.79
Felis leo (lion)	Non-avian	NSF	180.5	2.26
Galerella sanguinea (slender mongoose)	Non-avian	NSF	0.5875	-0.23
Giraffa camelopardalis (giraffe)	Non-avian	NSF	1010	3.00
Glyptemys muhlenbergii (turtle)	Non-avian	NSF	0.11	-0.96
Gorilla gorilla (gorilla)	Non-avian	KU	124	2.09

Homo sapiens (human)	Non-avian	KU	81	1.91
Hyaena hyaena (hyaena)	Non-avian	NSF	51.5	1.71
Hydrurga leptonyx (leopard seal)	Non-avian	NSF	400	2.60
Hylobates lar (gibbon)	Non-avian	KU	7.25	0.86
Lama glama (llama)	Non-avian	NSF	165	2.22
Lemur catta (lemur)	Non-avian	KU	2.2	0.34
Macaca mulatta (macaque)	Non-avian	KU	6.5	0.81
Mandrillus sphinx (mandrill)	Non-avian	KU	23.5	1.37
Mayailurus iriomotenis (iriomote cat)	Non-avian	KU	4.5	0.65
Meles meles (badger)	Non-avian	KU	10.05	1.00
Moloch horridus (thorny devil)	Non-avian	NSF	0.049	-1.31
Monachus tropicalis (monk seal)	Non-avian	NSF	160	2.20
Mus musculus (mouse)	Non-avian	NSF	0.1	-1.00
Otocyon megalotis (bat-eared fox)	Non-avian	NSF	4.15	0.62
Pan troglodytes (chimpanzee)	Non-avian	KU	48	1.68
Parahyaena brunnea (brown hyena)	Non-avian	NSF	42	1.62
Pogona vitticeps (bearded dragon)	Non-avian	NSF	0.475	-0.32
Pongo pygmaeus (orangutan)	Non-avian	KU	57.5	1.76
Procavia capensis (hyrax)	Non-avian	NSF	3.6	0.56
Python molurus (python)	Non-avian	NSF	38	1.58
Sphenodon punctatus (tuatara)	Non-avian	NSF	0.75	-0.12
Taxidea taxus (badger)	Non-avian	NSF	7.75	0.89
Ursus horribilis (grizzly bear)	Non-avian	NSF	367.5	2.57

Table S3: Distance matrices between species means (Procrustes above diagonal, Mahalanobis (D^2) below)

D2/Pr	Al	Ch	Du	Ge	Ha	Hu	Sq	Mo	Qu	Ra	Tu
Alligator	0.00	0.17	0.14	0.23	0.20	0.14	0.18	0.16	0.20	0.20	0.00
Chicken	15.97	0.00	0.10	0.27	0.22	0.13	0.19	0.12	0.24	0.19	15.97
Duck	14.21	8.79	0.00	0.22	0.21	0.12	0.16	0.07	0.18	0.17	14.21
Gerbil	17.23	22.00	17.62	0.00	0.19	0.25	0.14	0.25	0.14	0.26	17.23
Hamster	13.31	16.70	15.69	16.21	0.00	0.23	0.19	0.21	0.22	0.28	13.31
Human	13.66	10.29	9.89	20.93	16.22	0.00	0.19	0.14	0.20	0.15	13.66
Squamate	16.56	20.68	16.51	9.01	16.29	21.24	0.00	0.20	0.13	0.22	16.56
Mouse	14.59	9.45	6.80	21.19	17.20	9.77	20.66	0.00	0.21	0.16	14.59
Quail	15.16	20.95	16.38	8.98	15.49	19.36	10.63	18.98	0.00	0.24	15.16
Rat	16.58	15.49	12.64	21.12	20.60	13.62	19.64	11.98	20.25	0.00	16.58
Turtle	0.00	0.17	0.14	0.23	0.20	0.14	0.18	0.16	0.20	0.20	0.00

Table S4: Significance levels of distances between species means (Procrustes distances above diagonal, Mahalanobis distances (D^2) calculated from the Canonival Variates Analysis below)

D2/Pr	Al	Ch	Du	Ge	Ha	Hu	Sq	Mo	Qu	Ra	Tu
Alligator	-	0.001	0.000	0.008	0.006	0.002	0.000	0.001	0.162	0.001	-
Chicken	0.001	-	<.0001	0.003	0.001	0.001	0.001	0.000	0.128	0.000	0.001
Duck	0.000	<.0001	-	0.000	0.000	<.0001	<.0001	0.059	0.021	<.0001	0.000
Gerbil	0.009	0.001	0.000	-	0.065	0.001	0.042	0.002	1.000	0.002	0.009
Hamster	0.007	0.001	0.000	0.008	-	0.002	0.002	0.001	0.326	0.001	0.007
Human	0.002	0.001	<.0001	0.003	0.003	-	<.0001	0.002	0.045	0.000	0.002
Squamate	0.001	0.000	<.0001	0.003	0.002	0.000	-	0.000	0.087	<.0001	0.001
Mouse	0.001	0.000	<.0001	0.003	0.001	0.001	0.000	-	0.243	0.243	0.001
Quail	0.143	0.094	0.053	0.200	0.125	0.095	0.128	0.119	-	0.081	0.143
Rat	<.0001	0.000	<.0001	0.000	0.001	<.0001	<.0001	0.000	0.049	-	<.0001
Turtle	-	0.001	0.000	0.008	0.006	0.002	0.000	0.001	0.162	0.001	-